






THE PEAK FREQUENCY SOURCE OF SATURN'S KILOMETRIC RADIATION

L. Lamy^{1,2*} , R. Prangé¹ , M. Morooka³ ,
W. S. Kurth⁴ , and U. Taubenschuss⁵ 

* Corresponding author: laurent.lamy@lam.fr

Citation:

Lamy et al., 2023, The peak frequency source of Saturn's Kilometric Radiation, in *Planetary, Solar and Heliospheric Radio Emissions IX*, edited by C. K. Louis, C. M. Jackman, G. Fischer, A. H. Sulaiman, P. Zucca, published by DIAS, TCD, pp. 369–381, doi: 10.25546/103102

Abstract

In 2016–2017, the Cassini spacecraft explored the source regions of Saturn's Kilometric Radiation (SKR) within the kronian polar magnetosphere before ultimately plunging into the upper atmosphere of the planet. This powerful, non-thermal auroral radio emission analog to the Auroral Kilometric Radiation (AKR) at Earth, is radiated via the Cyclotron Maser Instability (CMI) by mildly relativistic electrons at frequencies close to the local electron gyrofrequency. The typical SKR spectrum ranges from a few kHz to ~ 1 MHz and thus corresponds to radiosources hosted along high latitude magnetic flux tubes from above the ionosphere up to a few kronian radii (R_S). During the F-ring orbital sequence, from Nov. 2016 to April 2017, Cassini probed the outer part of both northern and southern auroral regions, ranging in altitude from ~ 2.5 to $\sim 4 R_S$ above the atmosphere, and crossed several SKR low frequency (LF) sources (~ 10 – 30 kHz). A survey showed that the SKR LF sources strongly vary with time and local time, with the lowest frequencies being reached on the dawn sector. They were additionally colocated with the UV auroral oval and controlled by local time-variable magnetospheric electron densities, with important consequences on the use of SKR low frequency extensions as a proxy of magnetospheric dynamics. Along the final 22 proximal orbits, from April to 15th Sept. 2017, Cassini explored auroral altitudes below $2.5 R_S$ and crossed numerous deeper SKR sources at frequencies close to, or within, the emission peak frequency (~ 80 – 200 kHz). Here, we present a first survey of these proximal orbits, taking

¹ LESIA, Observatoire de Paris, Université PSL, CNRS, Sorbonne Université, Université de Paris, Meudon, France

² Aix Marseille Université, CNRS, CNES, LAM, Marseille, France

³ Swedish Institute of Space Physics, Uppsala, Sweden

⁴ Department of Physics and Astronomy, University of Iowa, Iowa City, USA

⁵ Department of Space Physics, Institute of Atmospheric Physics of the Czech Academy of Sciences, Prague, Czechia

advantage of observations of Saturn's UV aurorae by the Hubble Space Telescope coordinated with Cassini in situ radio and magnetic measurements. Understanding how the CMI operates in the widely different environments of solar system magnetospheres is important for the ongoing search of radio emissions from exoplanets, ultracool dwarves and active stars.

1 Introduction

Saturn's Kilometric Radiation (SKR) is a powerful non-thermal radio emission ranging from a few kHz to ~ 1 MHz, reminiscent of Auroral Kilometric Radiation (AKR) at Earth. After having been detected by the Voyager spacecraft in the early 1980s (Warwick et al., 1981; Kaiser et al., 1984), SKR was investigated at length during the 2004–2017 orbital tour of the Cassini mission, as recently reviewed in Lamy (2017, and references therein), thanks to quasi-continuous observations of its Radio and Plasma Wave Science (RPWS) experiment (Gurnett et al., 2004). The resemblance between SKR and AKR macroscopic properties – in terms of spectrum, dynamics, high degree of circular polarization or strongly oblique beaming – early led to postulate that the former was similarly radiated in Saturn's auroral regions by mildly relativistic electrons at frequencies f close to the local electron gyrofrequency f_{ce} through the Cyclotron Maser Instability (CMI) (Wu & Lee, 1979; Treumann, 2006, and references therein). The CMI resonance condition writes $\omega = \omega_{ce}/\Gamma + k_{//}v_{//}$ where $\omega = 2\pi f$ is the wave angular frequency, $\omega_{ce} = 2\pi f_{ce}$ is the electron Larmor angular frequency, Γ is the relativistic Lorentz factor and $k_{//}$ and $v_{//}$ are the projections of the wave \mathbf{k} vector and the electron velocity \mathbf{v} onto the direction of the magnetic field at the source. The CMI develops in highly magnetized/depleted plasma regions so that the ratio f_{ce}/f_{pe} , where f_{pe} is the electron plasma frequency, is low (Hilgers, 1992).

Still, the CMI scenario could only be validated in situ with radio, magnetic and electron measurements when Cassini unexpectedly flew by a southern SKR low frequency (LF) source at $f \sim 10$ kHz (~ 4 Saturn's radii – hereafter R_S – above the atmosphere) near 01:00 Local Time (LT) on day 2008–291 (Lamy et al., 2010; Mutel et al., 2010; Bunce et al., 2010; Kurth et al., 2011; Schippers et al., 2011; Lamy et al., 2011) and possibly by a second one at $f \sim 5$ kHz near 06:30 LT on day 2008–073 (Menietti et al., 2011). At both occasions, high cadence magnetic measurements providing f_{ce} were acquired by the MAG magnetometer (Dougherty et al., 2004) while the CAPS–ELS spectrometer provided electron distribution functions from 0.5 to 28 keV and the associated determination of f_{pe} (Linder et al., 1998). The combined analysis of those dataset revealed that the SKR source region is very similar to the AKR one. It is ~ 1000 – 2000 km wide and primarily radiates waves on the eXtraordinary (X) mode at frequencies $(f - f_{ce})/f_{ce}$ as low as -2% in regions where $f_{pe}/f_{ce} \sim 0.1$ which coincide with layers of upward field-aligned currents. The observed SKR flux density, growth rate and low frequency cutoff were found to be consistent with CMI-based predictions fed in by shell-type electron distribution functions with 6–9 keV characteristic energies observed simultaneously. A major difference with the terrestrial case, though, resided in the absence of large-scale auroral cavities. These are

however not necessary to achieve the low f_{pe}/f_{ce} ratios required by the CMI, Saturn's plasma density being already tenuous enough at high latitudes as the result of the fast planetary rotation (Lamy et al., 2010). Unfortunately, the CAPS-ELS spectrometer stopped operating in 2012, so that these two events remain to date the only cases during which electron distribution functions were measured directly within SKR sources.

During the early part of the Cassini Grand Finale, the spacecraft executed a series of 20 – so-called F-ring or ring-grazing – orbits (revolutions 251 to 270) between Nov. 2016 and Apr. 2017, during which the spacecraft sampled at multiple occasions the SKR LF source region with radio and magnetic measurements, only. A survey of those measurements revealed 3 additional dawnside SKR sources at $f \sim 13\text{--}23$ kHz (2.8 to 3.7 R_S above the atmosphere) in the north very similar to the southern ones (Lamy et al., 2018b). Namely, these were located between 09:00 and 10:30 LT, 300–6000 km wide, with $(f - f_{ce})/f_{ce}$ as low as -2% consistent with 6–12 keV shell-type source electrons, colocated with (i) upward currents and with (ii) regions where f_{pe} (as derived this time from Cassini/RPWS whistler mode emissions or Langmuir probe measurements) remained lower than $f_{ce}/10$. Conditions (i) and (ii) are both needed for the CMI to operate. A second major difference with the terrestrial case was revealed by comparing those measurements to Saturn's UV aurorae simultaneously imaged by the Hubble Space Telescope (HST Lamy et al., 2018a). If the observed SKR source region was found to map to the UV main oval, as expected, it surprisingly did not exactly coincide with it. We explained this partial correspondence by the fact that time-variable plasma densities encountered at such distances can yield too large values of f_{pe} for condition (ii) to be fulfilled so that the CMI can be quenched despite auroral energetic electrons being present. Also, Cassini did not encounter any southern source at similar frequencies on the dusk side, bringing evidence that the SKR spectrum is LT-dependent, with the lowest frequency (largest distance) emissions being reached on the dawn side.

In this follow-up work, we surveyed the 22 proximal orbits (revolutions 271 to 291) executed between Apr. 2017 and 15th Sept. 2017 to search for, and analyze, SKR sources at higher frequencies, up to the 100–400 kHz peak range, in both hemispheres. Investigating SKR emission produced close to this peak spectral range is interesting both to sample source regions closer to the planet and because these are likely more representative of the most efficient wave emission sites and associated electron acceleration processes. For the purpose of this study, we used Cassini radio and magnetic in situ measurements together with coordinated HST observations of the northern UV aurorae (Section 2), to achieve a list of source candidates (Section 3). We then validate and analyze the properties of two representative sources (Section 4).

2 Dataset

2.1 RPWS measurements

The RPWS instrument was equipped with a High Frequency Receiver (HFR) and a Wide-Band Receiver (WBR) which acquired complementary electric measurements, namely

survey time–frequency observations with 2– or 3–antennas and snapshots of waveform observations with 1 antenna (Gurnett et al., 2004). The HFR and WBR measurements and operation modes have been described in the appendix of Lamy et al. (2018b) and WBR high resolution dynamic spectra have been further described by Kurth et al. (2005); Fischer et al. (2022) for the study of SKR fine structures.

To adequately sample the SKR source region during the proximal orbits, HFR observations were generally acquired in 3–antenna mode above 30° . Indeed, the SKR polarization becomes strongly elliptical at high latitudes (Fischer et al., 2009), so that 3–antenna measurements (each made of a pair of 2–antenna measurements) are needed to retrieve the full Stokes parameters from a 3–antenna goniopolarimetric inversion (Cecconi & Zarka, 2005). At maximal time–frequency resolution, a scan of the 3.5 kHz to 16.125 MHz full HFR frequency range is typically achieved in 16 sec with a spectral resolution $\Delta f/f = 5\%$. Goniopolarimetric analysis of 3–antenna data is also necessary to perform reliable direction–finding and achieve images and polar projections of the magnetic footprint of SKR sources directly comparable to UV auroral polar projections (see Cecconi et al., 2009; Lamy et al., 2009, 2018b, for details and examples).

The WBR acquires waveform snapshots at the rate of 222,222 samples/s with 1 monopole or dipole antenna over the 0.8–75 kHz spectral range, which can be moved to high frequencies (HF) by using the HFR output. For the purpose of this study, we used WBR high resolution dynamic spectra built from Fast Fourier Transform of the signal using 2048 data points, yielding an effective time–frequency resolution of $1 \text{ sec} \times 109 \text{ Hz}$.

Finally, we used values of f_{pe} derived from RPWS/Langmuir probe measurements and values of f_{ce} together with magnetic field measurements derived from MAG observations.

2.2 HST images

Images of the northern UV aurorae of Saturn were acquired by HST with its Space Telescope Imaging Spectrograph (STIS) at regular intervals during the Cassini Grand Finale throughout 2017. Their timing was specifically chosen to match the expected encounters of the Cassini spacecraft with the SKR northern source region. Each image exposure time typically lasts for ~ 40 min. The full set of images, obtained near the northern solstice, providing the best visibility onto the northern polar region, has been analyzed in detail in Lamy et al. (2018a).

For the purpose of comparison with the Cassini measurements, we used processed polar projections accessible through the APIS service (Lamy et al., 2015).

3 Survey of the proximal orbits

The Cassini trajectory during the proximal orbits was such that the spacecraft successively traversed the northern auroral region at dawn and the southern auroral region at dusk for each revolution. Precisely, the predicted encounters with SKR sources ranged from 01:00 to 10:00 LT for the northern inbound leg and from 16:00 to 23:00 LT for the southern

outbound one, respectively (see Fig. S1 of Lamy et al., 2018b). We first inspected all the proximal orbits to identify plausible SKR sources, whenever the SKR low frequency cutoff f_{cut} visually appeared to stand below f_{ce} in survey RPWS/HFR observations. Indeed, in the absence of simultaneous measurements of the electron distribution function, events for which $f_{cut} > f_{ce}$ cannot be unambiguously considered as crossed sources. While $f_{cut} > f_{ce}$ emissions could for instance be produced by loss cone-driven CMI – as observed at Jupiter, see e.g. Collet et al. (2023) – they could alternately be produced by nearby, slightly distant, sources as we will show below.

Table 1: SKR sources plausibly crossed ($f \sim f_{ce}$) by Cassini during the proximal orbits.

Rev.	Day	f (kHz)	Hemisph.	RPWS	HST
271	2017–116	~ 80–100	North	HFR 3-ant + WBR	No
274	2017–135	~ 200–300	South	HFR 3-ant	No
275	2017–142	~ 15–100	North	HFR 3-ant + WBR	Yes
276	2017–148	~ 50–110	North	HFR 2-ant	No
277	2017–154	~ 30–120	North	HFR 2-ant	Yes (storm)
277	2017–155	~ 160–260	South	HFR 2-ant	No
279	2017–168	~ 170–220	South	HFR 3-ant + WBR	No
280	2017–174	~ 280–300	South	HFR 3-ant	No
281	2017–180	~ 100	South	HFR 3-ant	No
282	2017–187	~ 40–100	North	HFR 3-ant	Yes
282	2017–187	~ 120–220	South	HFR 3-ant	No
283	2017–193	~ 30–60	North	HFR 3-ant + WBR	No
284	2017–200	~ 100–130	North	HFR 3-ant	No
286	2017–213	~ 200–300	South	HFR 3-ant	No
287	2017–219	~ 100–130	North	HFR 3-ant	Yes
287	2017–219	~ 140–280	South	HFR 3-ant	No
288	2017–226	~ 20–140	North	HFR 3-ant + WBR	Yes (storm)
288	2017–226	~ 200–280	South	HFR 2-ant	No
289	2017–232	~ 80–160	North	HFR 3-ant + WBR	No
290	2017–239	~ 120	North	HFR 3-ant	Yes
290	2017–239	~ 220–300	South	HFR 2-ant	No
291	2017–245	~ 30–70	North	HFR 3-ant + WBR	No
292	2017–258	~ 100	North	HFR 2-ant	No

The list of events displayed in Table 1 provides the type of available RPWS measurements and indicates whenever coordinated HST observations were available. Overall, 13 (9 respectively) plausible SKR sources were crossed on the dawn (dusk) side at frequencies ranging from 15 to 160 kHz (100 to 300 kHz). In other words, southern duskside source candidates were less frequently encountered than northern dawnside ones, despite the former were closer to the SKR peak frequency. This confirms the strong LT dependence of the SKR spectrum with a larger extent (and therefore a larger spatial elongation of the source region toward larger distances) in the dawnside sector.

The value-added brought by coordinated HST observations and RPWS/HFR 3-antenna direction-finding analysis is illustrated in Figure 1 which shows three examples of (left) SKR dynamic spectra together with (right) polar projections of the northern UV aurorae

and of the northern/southern SKR footprints. For panels A₁ and C₁ (events on days 2017–154 and 187, which belong to Table 1), plausible SKR sources correspond to f_{cut} reaching f_{ce} and coincide with time intervals during which Cassini traversed the auroral flux tubes mapping to the auroral oval (the Cassini footpath is indicated by gray curves plotted on top of panels A₂ and C₂). On the contrary, for panel B₁ (day 174, excluded from Table 1),

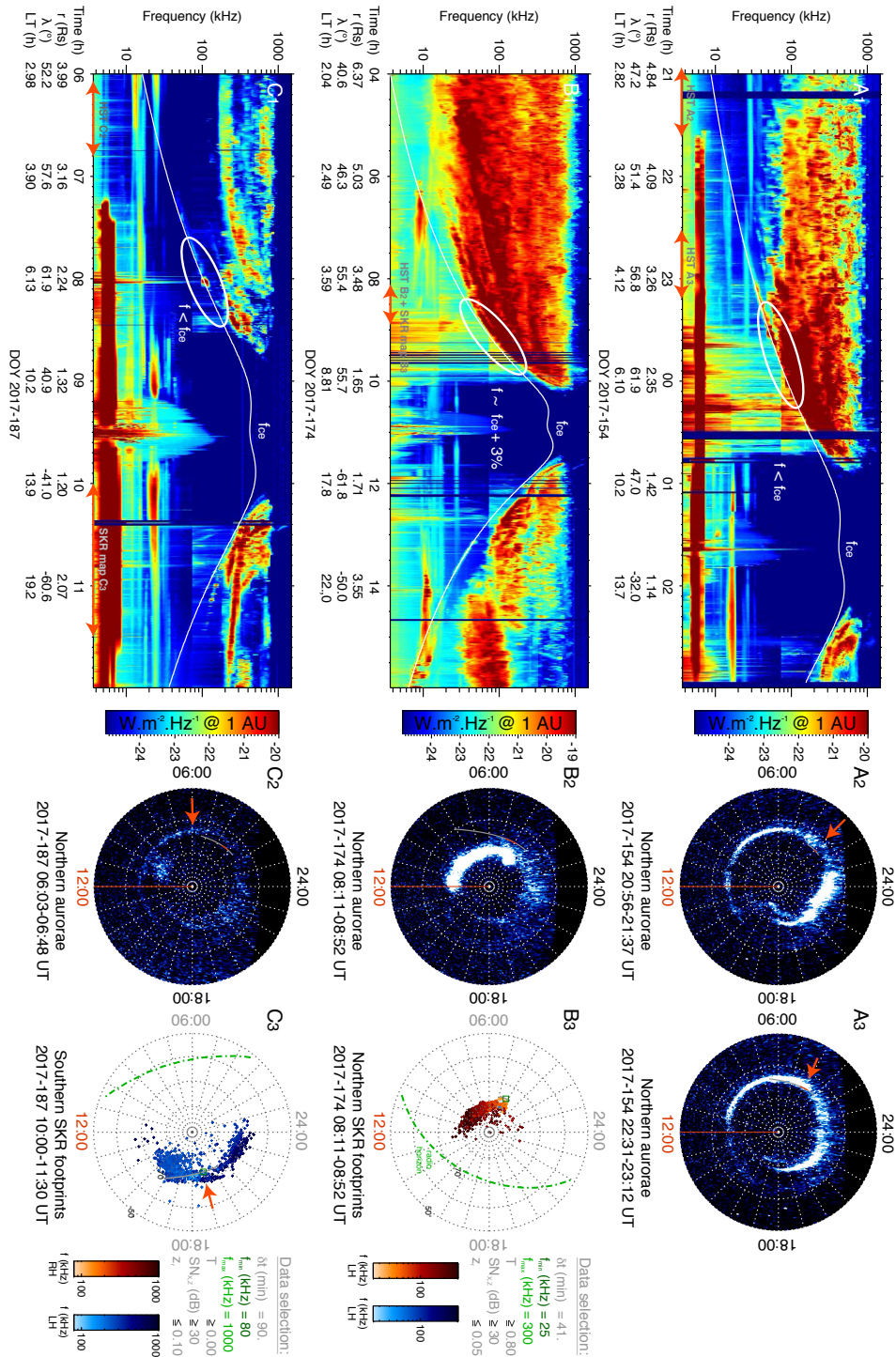


Figure 1: Caption on next page

Figure 1: (A_1 – B_1 – C_1) RPWS/HFR dynamic spectra. Plausible SKR sources correspond to LF emissions with $f \leq f_{ce}$ for the top (northern source) and bottom (northern and southern sources) panels, as opposed to the non-encounter displayed in the middle panel where $f \geq f_{ce}$. The double red arrows on the bottom x -axis mark the time interval of HST and SKR polar maps displayed on the right. ($A_{2,3}$ – B_2 – C_2) HST images of the northern UV aurorae (the indicated time interval is light-time travel corrected), where the red portion of the gray line maps the Cassini footpath strictly simultaneous to the HST exposure. (B_3 – C_3) Northern and southern polar projections of the SKR magnetic footprints derived from RPWS/HFR 3-antenna measurements. On the top and middle panels, the Cassini footpath traversed the flux tubes mapping to the northern UV aurorae or to the southern SKR footprints (as highlighted by red arrows). On the middle panel, the Cassini footpath remained far from the auroral oval.

f_{cut} remains slightly above f_{ce} while Cassini did not intercept at all any UV auroral flux tube. This event is an example of a strong UV auroral storm (panel B_2) accompanied by a global SKR intensification along colocated flux tubes (panel B_3) during which the auroral precipitations contracted toward the dawnside high latitudes. The inspection of the RPWS/WBR dynamic spectrum (not shown) shows that f_{cut} precisely reached $f_{ce} + 3\%$.

4 The cases of 2017–116 and 2017–154

To check quantitatively the validity of the $f_{cut} \leq f_{ce}$ condition and confirm/refine the identification of SKR sources, we applied the method developed by Lamy et al. (2010) to track f_{cut} from RPWS/HFR survey data. This method, which relies on the fitting of individual HFR spectra of the observed wave flux density by a model signal convoluted by the HFR filters, also improves the native spectral resolution. It is worth noting that, during the proximal orbits, the measured flux densities were often very high, regularly saturating the RPWS receivers and thus rendering the tracking of f_{cut} through this method difficult. We compared the obtained time series of f_{cut} with RPWS/WBR high resolution dynamic spectra whenever available. We sometimes found a fair correspondence between the two (as in Figure 3B of Lamy et al., 2018b), sometimes slightly larger f_{cut} in WBR dynamic spectra, barely reaching f_{ce} (not shown). We attribute this difference to the fact that WBR waveform measurements are acquired with 1 antenna, as opposed to HFR measurements using 3 antennas. As a result, the former remain sensitive to the wave direction and may be blind to close-in sources when the antenna direction is pointing near the source region. In other words, the low frequency envelope in the WBR dynamic spectra is likely to be an upper limit to the real value of f_{cut} .

Hereafter, we discuss two representative cases of SKR sources validated with this approach, one corresponding to standard SKR activity and one to intensified SKR coinciding with a UV auroral storm. Figures 2 and 3 show radio, plasma, and magnetic observations for northern SKR sources respectively encountered near 100 kHz and 30–80 kHz on days 2017–116 and 2017–154 (already shown in Figure 1, top) in the same format as Figures 1–2 from Lamy et al. (2018b). Lower frequencies (farther distances) are reached for the second, most active, episode. Both events show small-sized SKR HF X mode sources in panels A–B with $f_{cut} \leq f_{ce}$ (orange-shaded regions) in panels C, down to $f_{ce} - 2.5\%$. They correspond to plasma regions where $f_{pe}/f_{ce} \leq 0.1$, as shown in panels

D, permanently fulfilling CMI condition (ii). The limited temporal cadence of Langmuir probe measurements prevented tracking fine structures and possible small-scale cavities, though. Panels E confirm the coincidence of SKR sources with layers of upward cur-

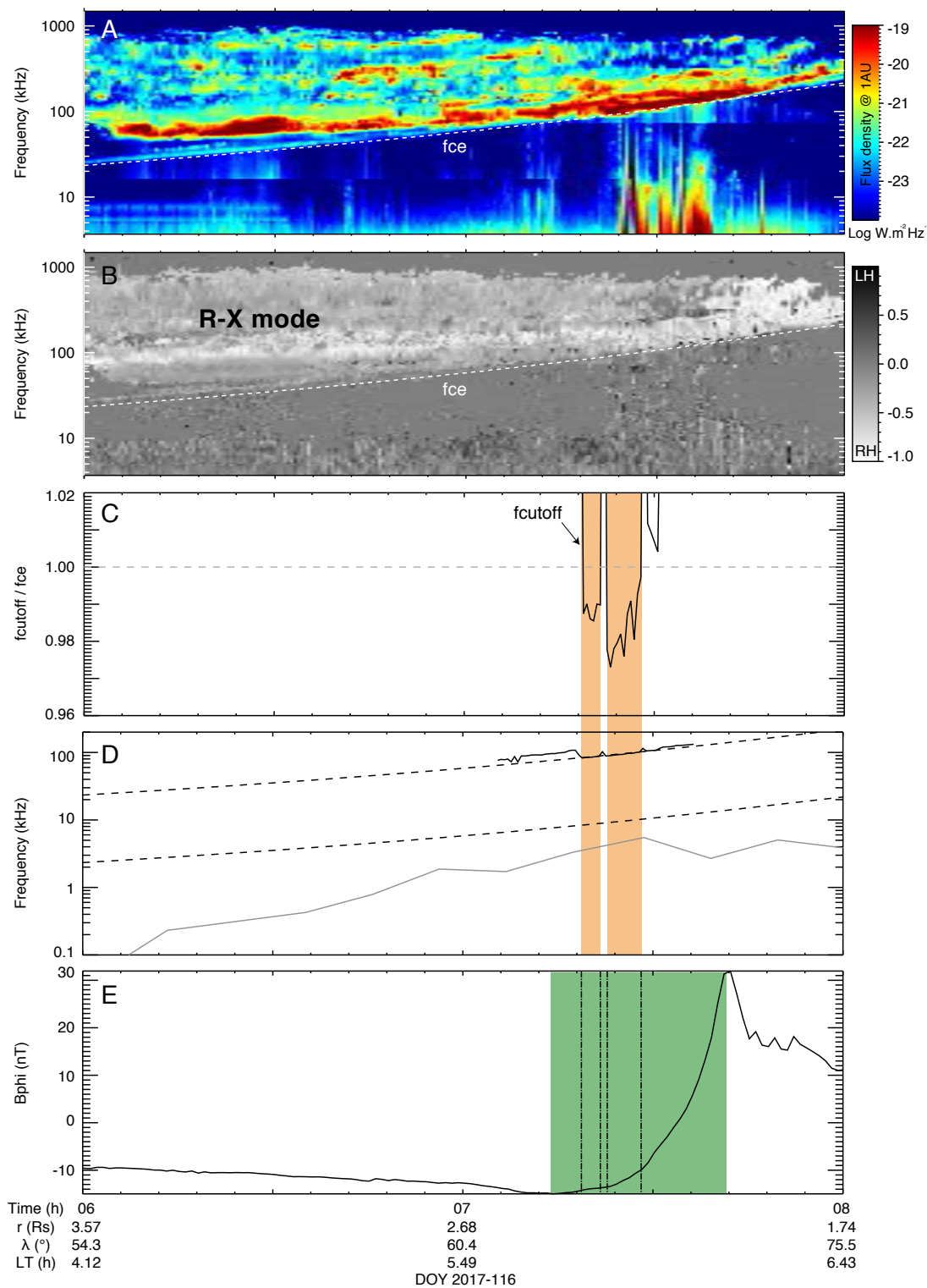


Figure 2: Caption on next page

Figure 2: Cassini radio, plasma, and magnetic field data acquired on day 2017–116 in the same format as Figures 1–2 in Lamy et al. (2018b). (A–B) Dynamic spectra of the wave flux density and degree of circular polarization. The white dashed lines indicate f_{ce} . X mode SKR with strong elliptical polarization is prominently observed throughout the interval. (C) Time series of the SKR low frequency cutoff (solid line), which falls strictly below f_{ce} during the orange–shaded intervals when f_{cut} was ~ 100 kHz. (D) Characteristic frequencies f_{cut} (solid black line), f_{ce} and $f_{ce}/10$ (dashed black lines) and f_{pe} (solid gray line). The ratio f_{pe}/f_{ce} remains ≤ 0.1 throughout the interval. (E) Azimuthal component of the magnetic field in spherical coordinates. The green–shaded area marks a region of positive slope of B_Φ , indicative of an upward–directed current region.

rent marked by green–shaded intervals, fulfilling CMI condition (i). The correspondence, however, is not perfect, which may indicate the intermittent presence of CMI–unstable energetic electrons within a broader upward field–aligned current region.

Assuming shell–type CMI–unstable electrons (the only source of free energy which can drive emission at frequencies strictly below f_{ce}), inverting the CMI resonance condition with $f = f_{cut}$ yields electron energies $E_{e-} = 7 \pm 3$ keV (varying within a 1.4–13.6 keV range) and $E_{e-} = 8 \pm 3$ keV (varying within a 0.4–16 keV range), respectively. Larger energies are therefore found farther from the planet for the second, most active, episode. Altogether, those values remain remarkably close to those obtained previously for LF sources at farther distances. They will bring further constraints to the dynamical efficiency and locus of acceleration processes generating those electron beams.

5 Conclusions and perspectives

In this study, we presented a first survey of the SKR sources observed in situ by Cassini near the SKR peak frequency with radio, plasma and magnetic in situ measurements during the proximal orbits, as a follow–up analysis of the SKR LF source region analyzed previously. We took benefit of coordinated HST images of the northern UV aurorae to monitor the auroral context and the encountered flux tubes. Overall, we achieved a list of plausible SKR sources with a low frequency cutoff $f_{cut} \leq f_{ce}$, ranging from 15 to 160 kHz (100 to 300 kHz) in the dawnside northern (duskside southern) hemisphere, respectively, which confirm the LT dependence of the SKR spectrum with the lower frequencies (farther distances) being reached on the dawn sector of the magnetosphere. We then measured the SKR low frequency cutoff with improved spectral resolution to track intervals where f_{cut} strictly lay below f_{ce} . We presented two representative illustrations of the auroral conditions and wave properties obtained for such SKR sources. Despite these two cases probing different, standard and active, SKR and auroral activity, they display remarkably similar properties, comparable to those derived for SKR LF sources. They correspond to small–sized X mode sources with f_{cut} as low as $f_{ce} - 2.5\%$, consistent with shell–driven CMI with electrons of 8 to 9 keV. The active SKR event corresponds to slightly larger electron energies observed at lower frequencies (farther along the flux tube). The surrounding auroral plasma is tenuous, with $f_{pe}/f_{ce} \leq 0.1$, and the sources are embedded within broader upward field–aligned currents. The correspondence between SKR sources and upward currents is not exact, suggesting that CMI–unstable electrons are not continuously encountered with such current layers. A statistical survey of the

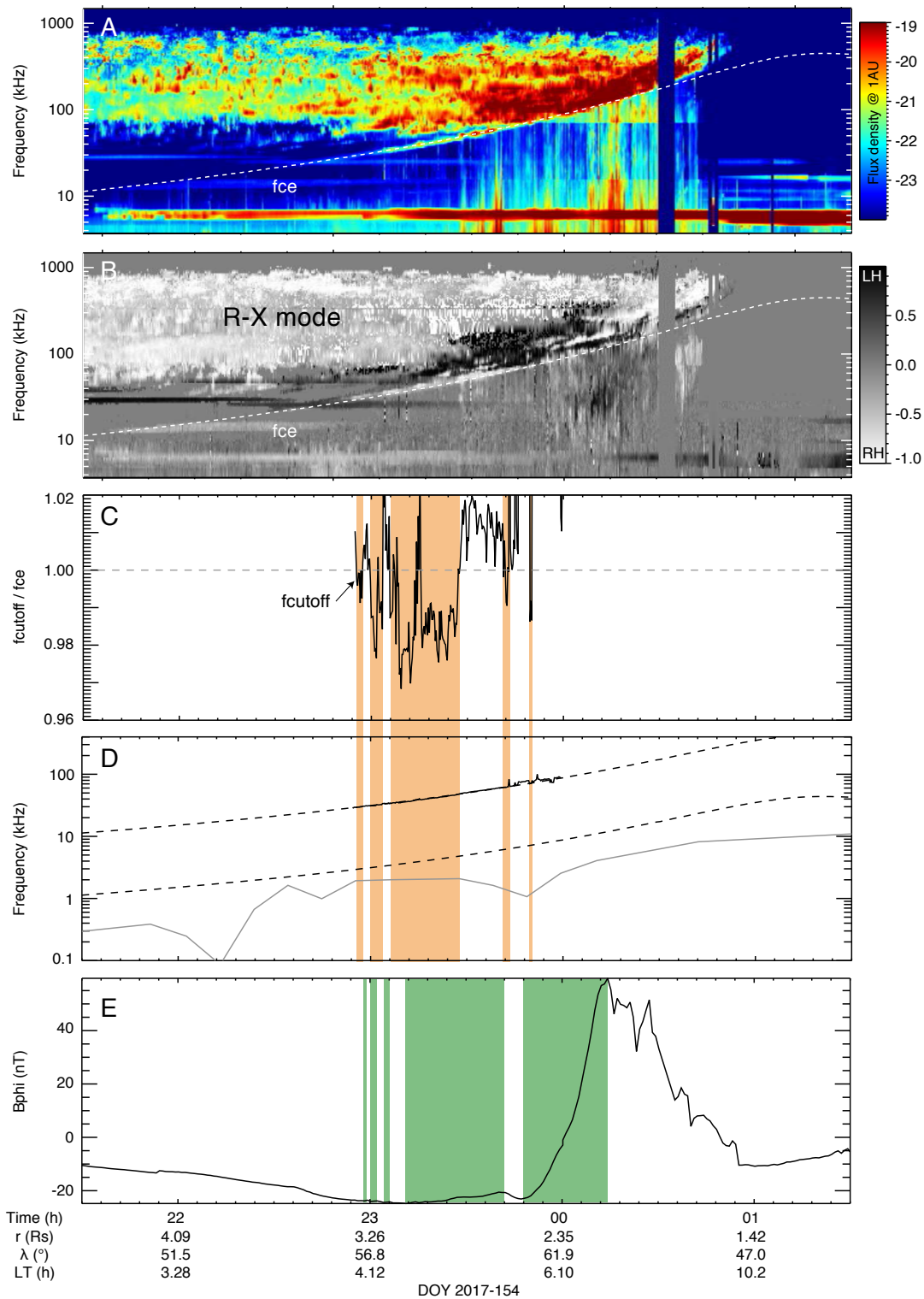


Figure 3: Same as Figure 2 for day 2017-154. The top panel was already shown in Figure 1, top.

full list of SKR HF sources, beyond the scope of this paper, will bring a more accurate average view on those first results.

Acknowledgements

The authors thank the referees for their valuable comments. The authors acknowledge support from CNES and from CNRS/INSU programs of Planetology (PNP) and Helio-physics (PNST). The Cassini RPWS and MAG raw data are accessible through the Planetary Data System at <https://pds-ppi.igpp.ucla.edu/mission/Cassini-Huygens>. The RPWS/HFR 2-antenna and 3-antenna data collections used in this study are referenced as Cecconi et al. (2017a,b) and are available through the LESIA-Kronos database at www.lesia.obspm.fr/kronos. The MAG data are referenced as Dougherty et al. (2019). The UV observations were obtained from the ESA-NASA Hubble Space Telescope (General Observer program 14811). The original data can be retrieved from the MAST archive at <http://archive.stsci.edu/hst/>, and the processed data from the APIS CNRS/INSU observation service <http://apis.obspm.fr> hosted by the Paris Astronomical Data Centre at Observatoire de Paris (Lamy & Henry, 2021).

References

- Bunce E. J., et al., 2010, Extraordinary field-aligned current signatures in Saturn's high-latitude magnetosphere: Analysis of Cassini data during Revolution 89, *Journal of Geophysical Research (Space Physics)*, 115, A10238
- Cecconi B., Zarka P., 2005, Direction finding and antenna calibration through analytical inversion of radio measurements performed using a system of two or three electric dipole antennas on a three-axis stabilized spacecraft, *Radio Science*, 40, RS3003
- Cecconi B., Lamy L., Zarka P., Prangé R., Kurth W. S., Louarn P., 2009, Goniopolarimetric study of the revolution 29 perikrone using the Cassini Radio and Plasma Wave Science instrument high-frequency radio receiver, *Journal of Geophysical Research (Space Physics)*, 114, A03215
- Cecconi B., Lamy L., Zarka P., 2017b, Cassini/RPWS/HFR LESIA/Kronos N3b Data Collection, doi:10.25935/F8NS-0911, <https://doi.org/10.25935/F8NS-0911>
- Cecconi B., Lamy L., Zarka P., 2017a, Cassini/RPWS/HFR LESIA/Kronos N3e Data Collection, doi:10.25935/9ZAB-FP47, <https://doi.org/10.25935/9ZAB-FP47>
- Collet B., Lamy L., Louis C. K., Zarka P., Prangé R., Louarn P., Sulaiman A., Kurth W. S., 2023, Characterization of Jupiter's decimetric radio sources: localization and new free energy source, in *Planetary, Solar and Helispheric Radio Emissions IX*, ed. C. K. Louis, C. M. Jackman, G. Fischer, A. H. Sulaiman, P. Zucca, DIAS, TCD, doi:10.25546/103095

- Dougherty M. K., et al., 2004, The Cassini Magnetic Field Investigation, *Sp. Sci. Rev.*, *114*, 331
- Dougherty M. K., Kellock S., Slootweg A. P., Achilleos N., Joy S. P., Mafi J. N., 2019, CASSINI ORBITER MAG CALIBRATED FULL RES V2.0 CO-E/SW/J/S-MAG-3-RDR-FULL-RES-V2.0, doi:10.17189/1521151, <https://doi.org/10.17189/1521151>
- Fischer G., et al., 2009, Elliptical polarization of Saturn Kilometric Radiation observed from high latitudes, *Journal of Geophysical Research (Space Physics)*, *114*, A08216
- Fischer G., Taubenschuss U., Piša D., 2022, Classification of spectral fine structures of Saturn kilometric radiation, *Annales Geophysicae*, *40*, 485
- Gurnett D. A., et al., 2004, The Cassini Radio and Plasma Wave Investigation, *Sp. Sci. Rev.*, *114*, 395
- Hilgers A., 1992, The auroral radiating plasma cavities, *Geophys. Res. Lett.*, *19*, 237
- Kaiser M. L., Desch M. D., Kurth W. S., Lecacheux A., Genova F., Pedersen B. M., Evans D. R., 1984, Saturn as a radio source, in *Saturn*, eds Gehrels, T. and Matthews, M. S., pp 378–415
- Kurth W. S., et al., 2005, High spectral and temporal resolution observations of Saturn kilometric radiation, *Geophys. Res. Lett.*, *32*, L20S07
- Kurth W. S., et al., 2011, A Close Encounter with a Saturn Kilometric Radiation Source Region, in *Planetary, Solar and Heliospheric Radio Emissions (PRE VII)*, eds Rucker, H. O. and Kurth, W. S. and Louarn, P. and Fischer, G., pp 75–85
- Lamy L., 2017, The Saturnian kilometric radiation before the Cassini Grand Finale, in *Planetary Radio Emissions VIII*, eds Fischer, G. and Mann, G. and Panchenko, M. and Zarka, P., pp 171–190, doi:10.1553/PRE8s171
- Lamy L., Henry F., 2021, APIS/HST data collection, doi:10.25935/T184-3B87, <https://doi.org/10.25935/T184-3B87>
- Lamy L., Cecconi B., Prangé R., Zarka P., Nichols J. D., Clarke J. T., 2009, An auroral oval at the footprint of Saturn's kilometric radio sources, colocated with the UV aurorae, *Journal of Geophysical Research (Space Physics)*, *114*, A10212
- Lamy L., et al., 2010, Properties of Saturn kilometric radiation measured within its source region, *Geophys. Res. Lett.*, *37*, L12104
- Lamy L., et al., 2011, Emission and propagation of Saturn kilometric radiation: Magnetoionic modes, beaming pattern, and polarization state, *Journal of Geophysical Research (Space Physics)*, *116*, A04212
- Lamy L., Prangé R., Henry F., Le Sidaner P., 2015, The Auroral Planetary Imaging and Spectroscopy (APIS) service, *Astronomy and Computing*, *11*, 138

- Lamy L., et al., 2018a, Saturn's Northern Aurorae at Solstice From HST Observations Coordinated With Cassini's Grand Finale, *Geophys. Res. Lett.*, *45*, 9353
- Lamy L., et al., 2018b, The low-frequency source of Saturn's kilometric radiation, *Science*, *362*, aat2027
- Linder D. R., et al., 1998, The Cassini CAPS Electron Spectrometer, *Geophysical Monograph Series*, *102*, 257
- Menietti J. D., Mutel R. L., Schippers P., Ye S. Y., Gurnett D. A., Lamy L., 2011, Analysis of Saturn kilometric radiation near a source center, *Journal of Geophysical Research (Space Physics)*, *116*, A12222
- Mutel R. L., et al., 2010, CMI growth rates for Saturnian kilometric radiation, *Geophys. Res. Lett.*, *37*, L19105
- Schippers P., et al., 2011, Auroral electron distributions within and close to the Saturn kilometric radiation source region, *Journal of Geophysical Research (Space Physics)*, *116*, A05203
- Treumann R. A., 2006, The electron-cyclotron maser for astrophysical application, *The Astron. & Astrophys. Rev.*, *13*, 229
- Warwick J. W., et al., 1981, Planetary Radio Astronomy Observations from Voyager 1 near Saturn, *Science*, *212*, 239
- Wu C. S., Lee L. C., 1979, A theory of the terrestrial kilometric radiation., *The Astrophys. J.*, *230*, 621